# Layer-Number-Dependent Antiferromagnetic and Ferromagnetic Behavior in $MnSb_2Te_4$

Zhihao Zang,[1,2] Yaozheng Zhu,[1] Ming Xi,[3] Shangjie Tian,[3] Tingting Wang,[1] Pingfan Gu,[1] Yuxuan Peng,[1] Shiqi Yang,[1,4] Xiaolong Xu,[1] Yanping Li,[1] Bo Han,[5,6] Liwei Liu,[7] Yeliang Wang,[7] Peng Gao,[2,5,6] Jinbo Yang,[1] Hechang Lei,[3,*] Yuan Huang,[7,†] and Yu Ye[1,2,8,‡]

[1]*State Key Laboratory for Mesoscopic Physics and Frontiers Science Center for Nano-optoelectronics, School of Physics, Peking University, Beijing 100871, China*
[2]*Collaborative Innovation Center of Quantum Matter, Beijing 100871, China*
[3]*Department of Physics and Beijing Key Laboratory of Opto-electronic Functional Materials and Micro-nano Devices, Renmin University of China, Beijing 100872, China*
[4]*Academy for Advanced Interdisciplinary Studies, Peking University, Beijing 100871, China*
[5]*International Center for Quantum Materials, School of Physics, Peking University, Beijing 100871, China*
[6]*Electron Microscopy Laboratory, School of Physics, Peking University, Beijing 100871, China*
[7]*Advanced Research Institute of Multidisciplinary Science, Beijing Institute of Technology, Beijing 100081, China*
[8]*Beijing Key Laboratory for Magnetoelectric Materials and Devices, Beijing 100871, China*

(Received 9 July 2021; revised 25 October 2021; accepted 29 November 2021; published 3 January 2022)

$MnBi_2Te_4$, an intrinsic magnetic topological insulator, has shown layer-number-correlated magnetic and topological phases. More interestingly, in the isostructural material $MnSb_2Te_4$, the antiferromagnetic (AFM) and ferromagnetic (FM) states have been both observed in the bulk counterparts, which are also predicted to be topologically nontrivial. Revealing the layer-number-dependent magnetic properties of $MnSb_2Te_4$ down to a single septuple layer (SL) is of great significance for exploring the topological phenomena. However, this is still elusive. Here, using the polar reflective magnetic circular dichroism spectroscopy, both the *A*-type AFM and FM behaviors are observed and comprehensively studied in $MnSb_2Te_4$ down to a single SL limit. In *A*-type AFM $MnSb_2Te_4$ flakes, an obvious odd-even layer-number effect is observed. An additional surface spin-flop (SSF) transition occurs in even-SL flakes with the number of layers larger than 2. With the AFM linear-chain model, we identify that the even-SL flakes stabilize in a collinear state between the SSF transition and the spin-flop transition due to their appropriate energy ratio between the magnetic-field-scale anisotropy and interlayer interaction. In FM $MnSb_2Te_4$ flakes, we observe very different magnetic behaviors with an abrupt spin-flipping transition and very small saturation fields, indicating a weakened interlayer interaction. By revealing the rich magnetic states of few-SL $MnSb_2Te_4$ on the parameter space of the number of layers, external magnetic field, and temperature, our findings pave the way for further quantum transport studies of few-SL $MnSb_2Te_4$.

DOI: 10.1103/PhysRevLett.128.017201

The interaction between topological states and magnetism leads to many fascinating quantum phenomena, such as the quantum anomalous Hall effect (QAHE) and the axion insulator state [1–4]. One of the most famous examples is the recently discovered layered intrinsic antiferromagnetic (AFM) topological insulator (TI), $MnBi_2Te_4$ [5–10]. *A*-type AFM coupling makes $MnBi_2Te_4$ exhibit evident odd and even layer-number magnetic state oscillations [11,12], and thus strongly layer-number-dependent band structure and topological phase [13,14]. As an isostructural material, the energy difference between the ferromagnetic (FM) and AFM states in ideal $MnSb_2Te_4$ is very small, so its magnetic property can be modulated through artificial methods. By changing the Mn/Sb site mixing, the magnetic properties of $MnSb_2Te_4$ can be tuned from AFM to FM [15,16]. Both the AFM and FM states in the bulk $MnSb_2Te_4$ have been observed and confirmed [17–22]. Moreover, recent first-principle calculations inferred that the $MnSb_2Te_4$ bulk is topologically nontrivial [16,23] and an experimental work found FM TI in $MnSb_2Te_4$ with Curie temperature ($T_C$) up to 45–50 K [17]. Comprehensively revealing the magnetic states of $MnSb_2Te_4$ under varying external magnetic fields, temperatures, and numbers of layers is of great significance for the further exploration of rich topological phenomena. However, to date, the layer-number-dependent magnetism of $MnSb_2Te_4$, either AFM or FM, remains elusive.

In this Letter, *A*-type AFM and FM behaviors in $MnSb_2Te_4$ are both observed to be maintained to a single septuple layer (SL). Using polar reflective magnetic circular dichroism (RMCD) spectroscopy, the magnetic evolution of few-SL $MnSb_2Te_4$ flakes under varying numbers of layers, external magnetic fields, and temperatures has been comprehensively studied. In *A*-type AFM–$MnSb_2Te_4$

 © 2022 American Physical Society

(MST) flakes, the obvious odd-even layer-number effect was observed. In odd-SL flakes, due to the uncompensated magnetic moment, a clear hysteresis loop centered at $\mu_0 H = 0$ T is observed, and a spin-flop transition occurs at a higher magnetic field. In even-SL flakes with $N \geq 4$, additional surface spin-flop (SSF) transitions occur. With the aid of the linear-chain model, the magnetic-field-scale anisotropy and interlayer interaction of $A$-type AFM $MnSb_2Te_4$ are determined, and the magnetic phase evolution under the external magnetic field is revealed. Therefore, we determine that the even-SL flakes stabilize in a collinear state after the SSF transition. In the FM-MST thin flakes, we observed very different magnetic behaviors showing an abrupt spin-flip transition and a very small saturation field (~0.1 T), indicating a weakened interlayer interaction. In thick FM flakes, the labyrinthine domain structures were observed at temperatures slightly lower than $T_C$. The rich magnetic states of few-SL $MnSb_2Te_4$ observed under different ground magnetic orders, numbers of layers, external magnetic fields, and temperatures are expected to explore the novel quantum phenomena.

As an isostructure to $MnBi_2Te_4$, $MnSb_2Te_4$ is a layered ternary telluride compound with a space group of $R\bar{3}m$, forming by stacking SL (Te-Sb-Te-Mn-Te-Sb-Te) with van der Waals (vdW) force [Fig. 1(a)], which is confirmed with a scanning transmission electron microscopy (STEM) measurement (Fig. S1 of the Supplemental Material [24]). From the perspective of crystal growth, $MnSb_2Te_4$ crystals are easy to grow in a wide growth window [15], which makes it possible to fine-tune the defect concentration and also makes the magnetic properties very sensitive to the growth. Here, we observe very different magnetic properties in two types of samples, namely, the AFM-MST and FM-MST ones, under different growth conditions (Part I of the Supplemental Material [24]). The Mn-Sb site-mixing ratios of these two samples are determined by carrying out single-crystal x-ray diffraction (SC XRD) [22,29,30].

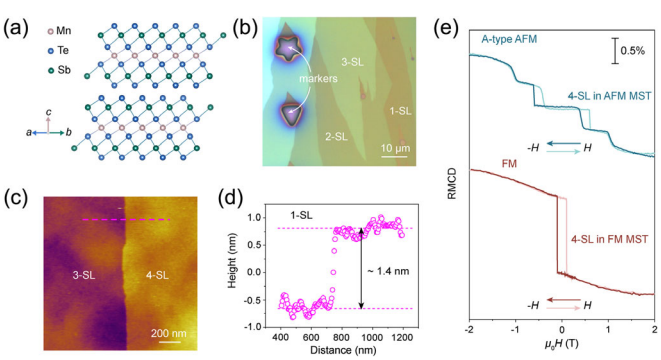


FIG. 1. (a) Crystal structure of $MnSb_2Te_4$. (b) The optical image of 1- and few-SL $MnSb_2Te_4$ flakes. (c) Height image of adjacent 3- and 4-SL $MnSb_2Te_4$ flakes. (d) Height line profile along with the magenta dashed line in (c). (e) RMCD signals versus external magnetic field of 4-SL flakes in AFM MST (upper) and FM MST (lower) measured at 2 K.

The refined SC-XRD data reveal 15% (20%) $Mn'_{Sb}$ (Mn atoms at Sb sites) and 25% (26%) $Sb^{\cdot}_{Mn}$ (Sb atoms at Mn sites) in AFM MST (FM MST) (Part III of the Supplemental Material [24]). The densities of $Mn'_{Sb}$ are further confirmed by scanning tunneling microscopy (STM) measurements (Fig. S2 of the Supplemental Material [24]). Owing to the existence of antisite defects, the Mn atoms in the Mn layer and Sb layer are suggested to be antiferromagnetically coupled and form ferrimagnetic orders in each SL [29–31]. This is also consistent with results of vibrating sample magnetometer (VSM) measurements (Fig. S3 of the Supplemental Material [24]), where the saturation moments are ~1.6 $\mu B$/Mn and ~1.9 $\mu B$/Mn for AFM MST and FM MST, respectively, much smaller than the expected ~4.7 $\mu B$/Mn from neutron scattering measurements [29].

Figure 1(b) shows a typical optical image of 1-SL to few-SL $MnSb_2Te_4$ flakes, where the hollow markers are used to locate the flakes to facilitate subsequent RMCD measurements. The layer number of $MnSb_2Te_4$ flake is further confirmed by atomic force microscopy characterizations (Fig. S4 of the Supplemental Material [24]). Figure 1(c) shows the height image of adjacent 3- and 4-SL flakes. The height line profile [Fig. 1(d)] shows that the step height between these two flakes is ~1.4 nm, which is consistent with the results of STEM (Fig. S1 of the Supplemental Material [24]). To detect the magnetic orders of few-SL $MnSb_2Te_4$ flakes, we collect the RMCD signals as a function of applied external magnetic field perpendicular to the sample plane. We use 0.25 $\mu$W, 633 nm HeNe laser as excitation with a spot size of ~2 $\mu$m. Figure 1(e) shows the RMCD signal evolution of 4-SL flake in both AFM MST and FM MST with the magnetic field at 2 K. The 4-SL flake in AFM MST exhibits a typical $A$-type AFM behavior, which shows the null net magnetic moment at $\mu_0 H = 0$ T and is followed by SSF and spin-flop transitions (discussed later). However, 4-SL flake in FM-MST shows typical FM behavior, which has a nonzero remanent magnetic moment at $\mu_0 H = 0$ T with a clear hysteresis loop and reaches the magnetic moment saturation state at a small field of ~0.1 T.

We then first studied the layer-number-dependent magnetic properties of AFM MST. Owing to the $A$-type antiferromagnetism, the odd- (even-) SL flakes have uncompensated (compensated) magnetic moments, and an odd-even layer-number effect should be expected. Figure 2(a) shows the RMCD evolution of 1-SL to 9-SL flakes under out-of-plane magnetic field sweeping back and forth from −2 to +2 T at 2 K. First, in odd-SL flakes, clear hysteresis loops centered at $\mu_0 H = 0$ T are observed due to the uncompensated magnetic moments. Second, as the magnetic field increases, odd-SL flakes (except for the 1-SL flake) undergo only one spin-flop transition [$\mu_0 H_{sf}^{odd}$, highlighted by the dashed blue curve in Fig. 2(a)] and finally evolve into complete out-of-plane magnetization,

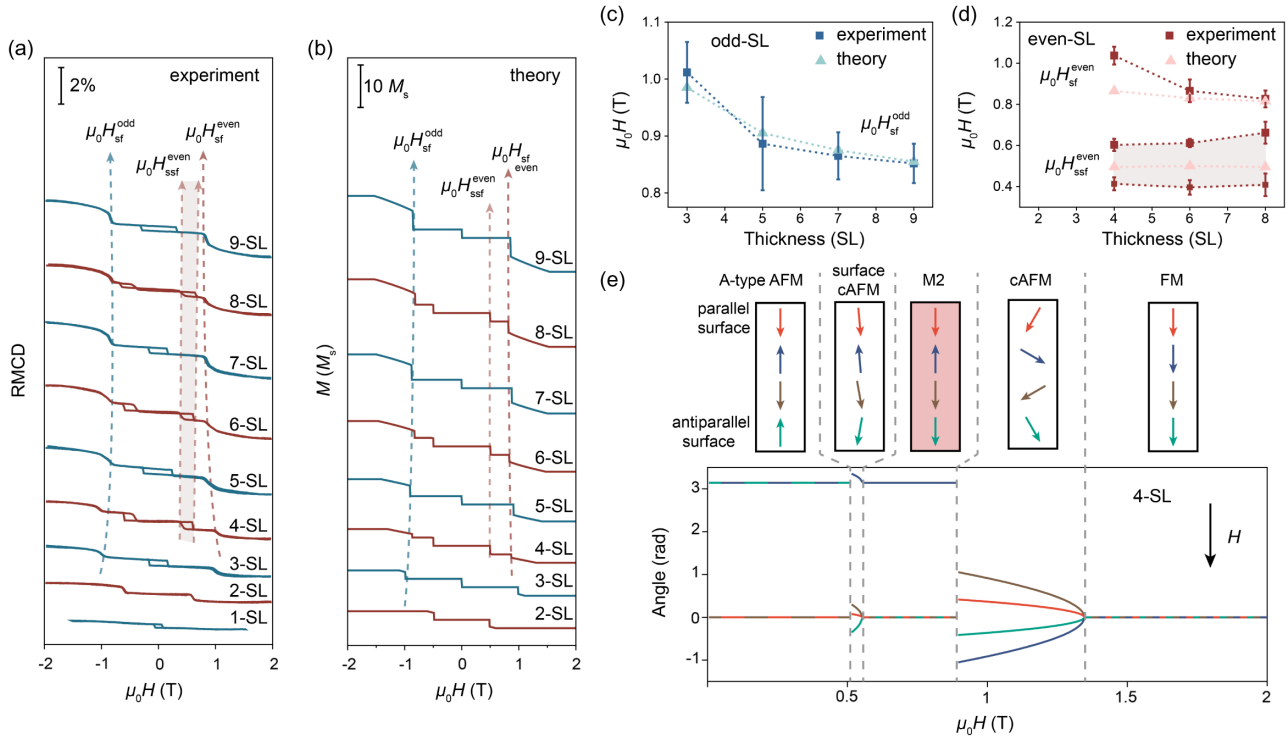


FIG. 2. (a) RMCD signals of 1- to 9-SL AFM-MST flakes measured at 2 K. (b) Calculated total magnetization of 2- to 9-SL flakes. (c) Extracted spin-flop fields and (d) SSF and spin-flop fields versus thickness for odd-SL and even-SL flakes. The squares with error bars and triangles denote experimental and calculated results, respectively. (e) Calculated magnetic state evolution of 4-SL flake under an external field. The upper (lower) panel denotes the spin configuration (angle of "macrospin" in each SL) at each state.

while even-SL (except for 2-SL flake) flakes undergo a two-step spin-flop transition [$\mu_0 H_{\rm ssf}^{\rm even}$ and $\mu_0 H_{\rm sf}^{\rm even}$, highlighted by the dashed red curves in Fig. 2(a)]. $\mu_0 H_{\rm sf}^{\rm odd}$ and $\mu_0 H_{\rm sf}^{\rm even}$ decrease with the increased number of layers, while $\mu_0 H_{\rm ssf}^{\rm even}$ is not sensitive to the number of layers. The values of $\mu_0 H_{\rm sf}^{\rm odd}$ are larger than those of $\mu_0 H_{\rm ssf}^{\rm even}$ because the extra Zeeman energy contributed by the uncompensated magnetic moment requires a higher field to overcome the total energy for odd-SL flakes. For even-SL flakes with $N \geq 4$, (1) a hysteresis loop can be found near $\mu_0 H_{\rm ssf}^{\rm even}$ [highlighted by the gray shaded area in Fig. 2(a)], indicating the existence of metastable states [32], and (2) a new magnetic state that is not sensitive to external magnetic fields appears between $\mu_0 H_{\rm ssf}^{\rm even}$ and $\mu_0 H_{\rm sf}^{\rm even}$, manifesting as a collinear state (labeled as the $M2$ state). The 1-SL flake shows an obvious FM behavior since there is only one layer with FM intralayer coupling, thus no spin-flop transition can occur [Fig. S5(a) of the Supplemental Material [24] ]. Besides, the magnetic behavior of a thick flake (~74 nm) is similar to that of the bulk sample characterized by VSM [Fig. S5(i) of the Supplemental Material [24] ].

To understand the magnetic evolution of $MnSb_2Te_4$ samples with different thicknesses, we use the AFM linear-chain model to elucidate how the magnetization and the angle of magnetic moments in each SL vary with the external field, where the spins in each SL is represented by a macrospin (see the details in previous reports [11]). Taking the magnetic-field-scale interlayer interaction, $H_J = (2J)/(\mu_0 M_s)$, and anisotropy, $H_K = K/(\mu_0 M_s)$, to be 1.03 and 0.42 T, respectively, the magnetization curves predicted by this model [Fig. 2(b)] coincide with the experimental data. For odd-SL flakes, the calculated $\mu_0 H_{\rm sf}^{\rm odd}$ value matches the extracted experimental value and decreases as the number of layers increases [Fig. 2(c)]. For even-SL flakes, the calculated $\mu_0 H_{\rm sf}^{\rm even}$ value also matches the experimental data, and the calculated $\mu_0 H_{\rm ssf}^{\rm even}$ value lays within the measured magnetic field range defined by the corresponding hysteresis loop [Fig. 2(d)].

The evolution of the macrospin in each SL under an external magnetic field graphically shows the process of the magnetic phase transition. For the 2-SL flake, the ground state at zero field is the AFM state ($\varphi_1 = \pi, \varphi_2 = 0$) and enters the noncollinear state [canted AFM (cAFM)] after the spin-flop field ($\varphi_1 = -\varphi_2$). Then, the spins fully align in the same direction when a large field is applied ($\varphi_1 = \varphi_2 = 0$) [Fig. S7(a) of the Supplemental Material [24] ]. For odd-SL flakes with $N \geq 3$, the magnetic moments in adjacent SLs are antiferromagnetically coupled at zero field, showing an uncompensated magnetization along the $c$ axis. When the applied field reaches $\mu_0 H_{\rm sf}^{\rm odd}$, the magnetic moments in each SL rotate coherently and the

flake enters the cAFM state. When the saturation field is reached, the magnetic moments fully align in the same direction [Figs. S7(b) and S7(c) of the Supplemental Material [24] ]. Unlike in odd-SL flakes, a two-step spin-flop transition occurs in even-SL flakes with $N \geq 4$. First, after the SSF transition at $\mu_0 H_{\mathrm{ssf}}^{\mathrm{even}}$, the system undergoes an obvious canting process near the antiparallel surface in the AFM state [surface cAFM; see the $N = 4$ case in Fig. 2(e) and $N = 6$ in Fig. S7(d) of the Supplemental Material [24] ], where parallel and antiparallel are defined as the direction of magnetization of the layer relative to the magnetic field. Similar SSF behavior was also observed in $MnBi_2Te_4$ [11,12]. However, unlike $MnBi_2Te_4$, after this cAFM state in $MnSb_2Te_4$, a new collinear state of total magnetization $M = 2M_s$ ($M2$) is observed, in which there are two more parallel SLs than antiparallel SLs. For $N = 4$, there is only one such $M2$ states [highlighted by the pink shaded area in Fig. 2(e)], where the magnetization of the outermost antiparallel SL layer is completely reversed, while the magnetization of other SLs remains unchanged ($\varphi_1 = \varphi_3 = \varphi_4 = 0$, $\varphi_2 = \pi$). For $N \geq 6$, there is more than one $M2$ state with exactly the same energy (Part VIII of the Supplemental Material [24]). We note that, compared with $MnBi_2Te_4$, the $H_K/H_J$ ratio of $MnSb_2Te_4$ is slightly larger, which stabilizes the appearance of these $M2$ states. A recent computational work concluded that the $H_K/H_J$ ratio of $MnBi_2Te_4$ is very close to the critical value for the appearance of such collinear $M2$ states [32]. Then, after the spin-flop transition at $\mu_0 H_{\mathrm{sf}}^{\mathrm{even}}$, the magnetic moments of each SL start to rotate symmetrically (the cAFM state), and the system finally enters the FM state when the applied field is large enough [Fig. 2(e)].

Then, we studied the magnetic properties of FM-MST flakes with different thicknesses. Unlike the slanted hysteresis loop observed in the bulk crystal [Fig. S3(d) of the Supplemental Material [24] ] clear rectangular hysteresis loops with vertical jumps are observed in the exfoliated flakes down to 1 SL [Fig. 3(a) of the Supplemental Material [24] ], indicating the FM orders with large out-of-plane anisotropy. No clear layer-number dependence presents and the coercive field of 1- to 5-SL flakes is ~0.1 T, slightly larger than that of bulk flake (~0.08 T). The enhanced coercive fields of thin flakes can be attributed to the enhanced out-of-plane anisotropy and reduced screening effect, which has been observed in other two-dimensional magnetic systems [33,34]. Notably, the magnetic behaviors shown for all the exfoliated flakes with different thicknesses reveal the domination of single-domain behavior at 2 K, distinct from the bulk crystal [Fig. S3(d) of the Supplemental Material [24] ], which is a typical multi-domain behavior [20]. The observation and confirmation of FM states in $MnSb_2Te_4$ under the two-dimensional limit provide an ideal platform to study the topological quantum phenomena.

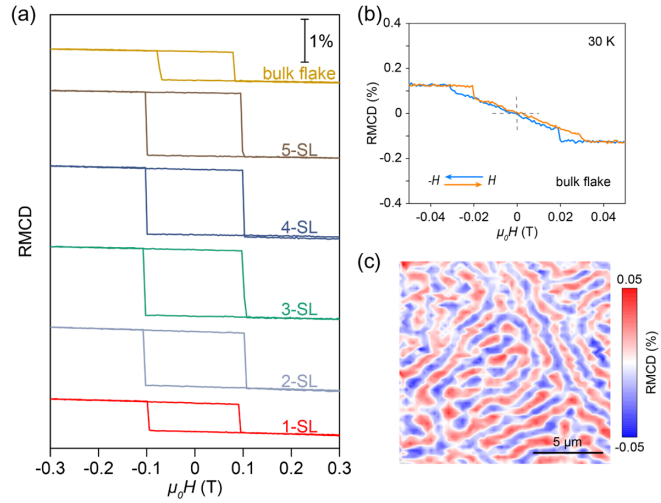


FIG. 3. (a) RMCD signals of 1- to 5-SL thin flakes and bulk flake in FM MST measured at 2 K. (b) RMCD signals of the bulk flake measured at 30 K. (c) Spatial RMCD map of the bulk flake at 30 K with zero field, as indicated by the gray dashed cross in (b).

Interestingly, magnetic properties of the exfoliated bulk flake (~560 nm) are also dominated by single-domain behavior at 2 K [Fig. 3(a)]. Although, unlike with the thin flakes, its rectangular hysteresis loop persists only to ~10 K, while the hysteresis vanishes at ~34 K [Fig. S8 (e) of the Supplemental Material [24] ]. In the intermediate temperature range (10–34 K), multiple magnetic transitions occur. For example, at 30 K [Fig. 3(b)], when the field is swept upward, the RMCD signal jumps abruptly at a negative field to an intermediate level, increases linearly across zero at 0 T, and finally reaches saturation. The downward sweeping shows time-reversal magnetic behavior. Similar phenomena have been reported in other systems, like $Fe_3GeTe_2$ thick flakes and Co/Pt multilayer films, revealing the formation of labyrinthine domain structures [35–37]. To confirm the domain structure, the RMCD mapping was conducted at 30 K and $\mu_0 H = 0$ [with a zero net RMCD signal marked in Fig. 3(b)], in which clear labyrinthine domain structures with a typical domain width of ~625 nm were observed [Fig. 3(c)].

To elucidate the critical temperatures of AFM MST and FM MST, we measured their RMCD signals with different layer numbers at varying temperatures. For 4-SL AFM-MST flake, with temperature increasing, the hysteresis loop near the $\mu_0 H_{\mathrm{ssf}}^{\mathrm{even}}$ shrinks and eventually disappears, and the spin-flop transition at $\mu_0 H_{\mathrm{sf}}^{\mathrm{even}}$ smears out at the Néel temperature ($T_N$) ~18.5 K [see Fig. 4(a) and also Fig. S5 of the Supplemental Material [24] ]. As the temperature increases, the spin-flop field decreases because the magnetic anisotropy $K$ decreases with increasing magnetic fluctuation [38,39]. For 4-SL FM-MST flake, the rectangular hysteresis loop is observed at all measured temperatures below $T_C$, shrinks as the temperature rises,

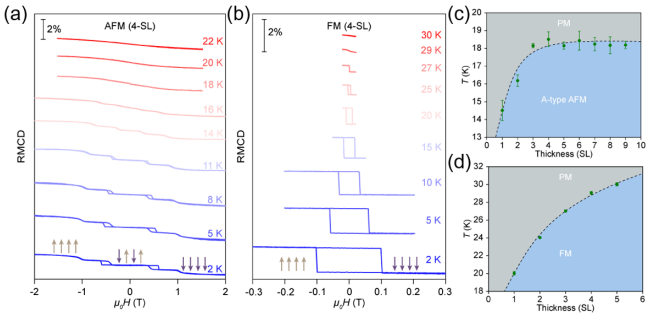


FIG. 4. Temperature-dependent RMCD results of 4-SL flakes in (a) AFM MST and (b) FM MST. Thickness-temperature phase diagrams of (c) AFM MST and (d) FM MST. The error bars are the uncertainties and the black dashed lines denote the phase boundaries.

and eventually disappears at ~27 K [see Fig. 4(b) and also Fig. S8 of the Supplemental Material [24] ]. The measured $T_C$ in 4-SL FM MST is higher than $T_N$ of 4-SL AFM MST. With that, we constructed the temperature-field diagrams of 3- and 4-SL AFM MST and FM MST [Fig. S9 of the Supplmental Material [24] ]. For AFM MST, two ($A$-type AFM/cAFM and cAFM/FM; brown dashed lines) and three ($A$-type AFM/$M2$, $M2$/cAFM, and cAFM/FM; brown dashed lines) phase boundaries can be determined in 3- and 4-SL flakes, respectively. For FM MST, only one phase boundary (spin-up/spin-down; brown dashed line) can be determined since only spin-flip occurs in the FM MST. By using the critical power law $A(1 - T/T_{\mathrm{critical}})^{\beta}$ ($T_{\mathrm{critical}}$: $T_N$ in AFM MST and $T_C$ in FM MST) [37], we obtained $T_{\mathrm{critical}}$ for all the flakes and constructed the thickness-temperature phase diagrams [Figs. 4(c) and 4(d)]. For AFM MST, the phase boundary between the AFM and paramagnetic (PM) states can be identified [Fig. 4(c)]. The $T_N$ of 1-SL (14.5 K) and 2-SL (16.2 K) flakes are smaller than that of the thicker samples (~18 K), which may be caused by the increased thermal fluctuation and disappearance of interlayer coupling. For FM MST, the phase boundary between the FM and PM states can be identified. Relative to the $T_N$ in AFM MST, a higher $T_C$ is obtained in FM MST and increases with the number of layers, approaching the value of bulk crystal in the thicker flakes.

In summary, we have observed both layer-number-dependent $A$-type AFM and FM behaviors in $MnSb_2Te_4$, which indicates that the magnetic phase of the $MnSb_2Te_4$ is very sensitive to the growth condition. The sensitive magnetic states in $MnSb_2Te_4$ few-SL flakes also advise the necessary magneto-optical measurement before transport measurement. Clear SSF transitions and stable $M2$ collinear states are obtained in the even-SL flakes with $N \geq 4$, which enriches the $A$-type vdW AFM material family and provides unprecedented opportunities to study the novel quantum effect of $MnSb_2Te_4$ correlating with these magnetic states. In the QAHE, the FM interlayer coupling is preferable so that dissipationless transport can be realized at zero field. The observation of FM states in $MnSb_2Te_4$ down to single SL provides an ideal platform to clarify the topology of $MnSb_2Te_4$ and further study the topological quantum phenomena, e.g., QAHE.

This work was supported by the National Key R&D Program of China (Grants No. 2018YFA0306900, No. 2017YFA0206301, and No. 2019YFA0308000), the National Natural Science Foundation of China (Grants No. 615210045, No. 11822412, No. 62022089, No. 11874405, No. 52125307, and No. 11774423), and Beijing Natural Science Foundation (Grant No. Z200005). The authors acknowledge the Electron Microscopy Laboratory at Peking University for the use of electron microscopes. Y. Y. and Z. Z. conceived the project. Z. Z. performed the measurements. Y. Z. performed the theoretical models and calculations. Z. Z., Y. Z., and Y. Y. analyzed the data and wrote the manuscript. Y. H. prepared the samples. M. X., S. T., and H. L. grew the $MnSb_2Te_4$ bulk crystals. T. W. performed the AFM measurements. L. L. and Y. W. performed the STM measurements. B. H. and P. Gao performed the STEM measurements. P. Gu, Y. P., S. Y., X. X., and J. Y. participated in the discussion. All authors discussed the results and contributed to the manuscript.

*hlei@ruc.edu.cn
†yhuang@bit.edu.cn
‡yeyu@pku.edu.cn

[1] Y. Tokura, K. Yasuda, and A. Tsukazaki, Nat. Rev. Phys. **1**, 126 (2019).
[2] C.-Z. Chang *et al.*, Science **340**, 167 (2013).
[3] R. Yu, W. Zhang, H.-J. Zhang, S.-C. Zhang, X. Dai, and Z. Fang, Science **329**, 61 (2010).
[4] M. Mogi, M. Kawamura, R. Yoshimi, A. Tsukazaki, Y. Kozuka, N. Shirakawa, K. Takahashi, M. Kawasaki, and Y. Tokura, Nat. Mater. **16**, 516 (2017).
[5] J.-Q. Yan, Q. Zhang, T. Heitmann, Z. Huang, K. Y. Chen, J.-G. Cheng, W. Wu, D. Vaknin, B. C. Sales, and R. J. McQueeney, Phys. Rev. Mater. **3**, 064202 (2019).
[6] M. M. Otrokov *et al.*, Nature (London) **576**, 416 (2019).
[7] M. M. Otrokov *et al.*, 2D Mater. **4**, 025082 (2017).
[8] Y. Deng, Y. Yu, M. Z. Shi, Z. Guo, Z. Xu, J. Wang, X. H. Chen, and Y. Zhang, Science **367**, 895 (2020).
[9] C. Liu, Y. Wang, H. Li, Y. Wu, Y. Li, J. Li, K. He, Y. Xu, J. Zhang, and Y. Wang, Nat. Mater. **19**, 522 (2020).
[10] J. Ge, Y. Liu, J. Li, H. Li, T. Luo, Y. Wu, Y. Xu, and J. Wang, Natl. Sci. Rev. **7**, 1280 (2020).
[11] S. Yang *et al.*, Phys. Rev. X **11**, 011003 (2021).
[12] D. Ovchinnikov *et al.*, Nano Lett. **21**, 2544 (2021).
[13] M. M. Otrokov, I. P. Rusinov, M. Blanco-Rey, M. Hoffmann, A. Y. Vyazovskaya, S. V. Eremeev, A. Ernst, P. M. Echenique, A. Arnau, and E. V. Chulkov, Phys. Rev. Lett. **122**, 107202 (2019).
[14] J. Li, Y. Li, S. Du, Z. Wang, B.-L. Gu, S.-C. Zhang, K. He, W. Duan, and Y. Xu, Sci. Adv. **5**, eaaw5685 (2019).
[15] Y. Liu *et al.*, Phys. Rev. X **11**, 021033 (2021).

[16] L. Zhou, Z. Tan, D. Yan, Z. Fang, Y. Shi, and H. Weng, Phys. Rev. B **102**, 085114 (2020).
[17] S. Wimmer *et al.*, Adv. Mater. **33**, 2102935 (2021).
[18] J.-Q. Yan, S. Okamoto, M. A. McGuire, A. F. May, R. J. McQueeney, and B. C. Sales, Phys. Rev. B **100**, 104409 (2019).
[19] G. Shi, M. Zhang, D. Yan, H. Feng, M. Yang, Y. Shi, and Y. Li, Chin. Phys. Lett. **37**, 047301 (2020).
[20] W. Ge, P. M. Sass, J. Yan, S. H. Lee, Z. Mao, and W. Wu, Phys. Rev. B **103**, 134403 (2021).
[21] P. M. Sass, W. Ge, J. Yan, D. Obeysekera, J. Yang, and W. Wu, Nano Lett. **20**, 2609 (2020).
[22] H. Li, Y. Li, Y. Lian, W. Xie, L. Chen, J. Zhang, Y. Wu, and S. Fan, Sci. China Mater. 1 (2021), 10.1007/s40843-021-1738-9.
[23] S. Eremeev, I. Rusinov, Y. M. Koroteev, A. Y. Vyazovskaya, M. Hoffmann, P. Echenique, A. Ernst, M. Otrokov, and E. Chulkov, J. Phys. Chem. Lett. **12**, 4268 (2021).
[24] See Supplemental Material at http://link.aps.org/supplemental/10.1103/PhysRevLett.128.017201, which includes Refs. [25–28], for (I) the method of single-crystal growth, (II) STEM measurements of AFM MST and FM MST, (III) single-crystal XRD results of AFM MST and FM MST, (IV) STM measurements of AFM MST and FM MST, (V) VSM results of AFM-MST and FM-MST bulk crystals, (VI) optical images and height profiles of exfoliated flakes in AFM MST, (VII) temperature-dependent RMCD results for flakes with different thicknesses in AFM MST, (VIII) discussions on collinear states in even-SL flakes in AFM MST, (IX) calculated angle evolution of other few-SL flakes in AFM MST, (X) temperature-dependent RMCD results for flakes with different thicknesses in FM MST, and (XI) temperature-field phase diagrams of few-SL flakes in AFM MST and FM MST.
[25] Y. Yuan *et al.*, Nano Lett. **20**, 3271 (2020).
[26] Z. Huang, M.-H. Du, J. Yan, and W. Wu, Phys. Rev. Mater. **4**, 121202(R) (2020).
[27] L. Ding, C. Hu, F. Ye, E. Feng, N. Ni, and H. Cao, Phys. Rev. B **101**, 020412(R) (2020).
[28] P. M. Sass, J. Kim, D. Vanderbilt, J. Yan, and W. Wu, Phys. Rev. Lett. **125**, 037201 (2020).
[29] D. Y. Yan, M. Yang, P. B. Song, Y. T. Song, C. X. Wang, C. J. Yi, and Y. G. Shi, Phys. Rev. B **103**, 224412 (2021).
[30] T. Murakami, Y. Nambu, T. Koretsune, G. Xiangyu, T. Yamamoto, C. M. Brown, and H. Kageyama, Phys. Rev. B **100**, 195103 (2019).
[31] Y. Lai, L. Ke, J. Yan, R. D. McDonald, and R. J. McQueeney, Phys. Rev. B **103**, 184429 (2021).
[32] C. Lei, O. Heinonen, A. H. MacDonald, and R. J. McQueeney, Phys. Rev. Mater. **5**, 064201 (2021).
[33] W. Jin *et al.*, Nat. Commun. **9**, 5122 (2018).
[34] Y. Peng *et al.*, Adv. Funct. Mater. **30**, 1910036 (2020).
[35] M. S. Pierce *et al.*, Phys. Rev. Lett. **94**, 017202 (2005).
[36] E. A. Jagla, Phys. Rev. B **72**, 094406 (2005).
[37] Z. Fei *et al.*, Nat. Mater. **17**, 778 (2018).
[38] A. Tan, V. Labracherie, N. Kunchur, A. U. B. Wolter, J. Cornejo, J. Dufouleur, B. Büchner, A. Isaeva, and R. Giraud, Phys. Rev. Lett. **124**, 197201 (2020).
[39] Y. Peng *et al.*, Adv. Mater. **32**, 2001200 (2020).